Unified Distributed Control of Grid-Forming and Grid-Feeding Converters in DC Microgrids with Average Voltage Regulation and Current Sharing

Sheik M. Mohiuddin and Junjian Qi
Department of Electrical and Computer Engineering
Stevens Institute of Technology
Hoboken, NJ 07030 USA
smohiudd@stevens.edu; jqi8@stevens.edu

***Abstract*—This paper proposes a unified distributed secondary control for the grid-forming (GFM) and grid-feeding (GFE) converters in DC microgrids. An optimization problem is formulated for the secondary control and the objective function considers regulating the global average of the GFM and GFE converter output voltages and proportional current sharing among all GFM and GFE converters. A unified distributed control is then designed to generate voltage and current references respectively for GFM and GFE converters based on the formulated optimization problem. The dynamic model of the DC microgrid under the proposed control is also developed, and steady-state analysis is performed to show that the proposed distributed control can achieve the control objectives in steady state. The performance of the proposed control is validated through real-time simulations in OPAL-RT on an 8-DG DC microgrid system.**

***Index Terms*—Current sharing, DC microgrid, distributed control, grid-feeding converter, grid-forming converter, voltage regulation.**

I. Introduction

With the increased penetration of renewable energy and energy storage, DC microgrid is gaining popularity due to the elimination of redundant DC-AC conversion, improved reliability, and high efficiency [1], [2]. DC microgrid can either operate independently or coexist with the AC system. DC microgrid does not encounter the traditional challenges such as reactive power support, frequency synchronization, transformer inrush current, and harmonic issues [3].

DC microgrid can accommodate different types of sources such as PV, wind, and energy storage that are usually connected to the DC bus through power electronic interfaces. Depending on the nature of the sources, the DC-DC converters can operate in grid-forming (GFM) or grid-feeding (GFE) mode [4], [5]. In GFM mode the DC converters regulate the distributed generator (DG) output voltages whereas in GFE mode the converters inject constant power into the DC microgrid. A DC microgrid with converters operating in both GFM and GFE modes can provide better voltage regulation, modularity, and expandability [2], [4].

For the regulation of parallel-connected DC-DC converters, droop-based primary controllers have been proposed for voltage stabilization and current sharing [6]. However, in the presence of nonlinear loads, line impedance mismatches, and measurement noises the droop control provides poor voltage regulation and current sharing [7]–[9]. To solve this problem the secondary control with centralized or distributed structure is proposed [10]. The centralized control suffers from the single point of failure problem [1]. By contrast, the distributed control that utilizes a sparse communication network can lead to improved reliability, lower computational complexity, reduced cost, and scalability [7], [11], [12].

The utilization of GFM and GFE converters from energy management perspective has been considered in [5]. In [13], the stability of a DC microgrid with GFM and GFE converters is studied. The authors in [2] present a decentralized droop control for DC microgrids. However, the droop control has the aforementioned limitations and gives inappropriate voltage/current regulation. In [4], a communication based droop control is proposed for GFM and GFE converters. However, this control only considers the average voltage of the GFM DGs, and the current sharing among all DGs is not included in the control design. For the appropriate control of the microgrid average voltage, information from all DGs needs to be considered. Also, proportional current sharing needs to be achieved among all GFM and GFE converters as inappropriate current sharing may overload some of the converters and lead to thermal stress on the converter switches.

In this paper, we propose a unified distributed control for both GFM and GFE converters in DC microgrids to achieve average voltage regulation and current sharing among all GFM and GFE converters utilizing a single communication network. Although a unified distributed control of GFM and grid-following inverters has been proposed for AC microgrid system [10], the control approach remains unexplored for DC microgrids. Also, in [10] the dynamic model is not developed and only Simulink simulation results are presented. The main contributions of this paper can be summarized as follows.

1) A unified distributed control is proposed for both GFM and GFE converters in DC microgrids. The proposed control is designed based on a formulated optimization problem where the regulation of global average voltage

This work was supported by the National Science Foundation under Grant No. ECCS-2103426.

among the GFM and GFE converters and achieving proportional current sharing among them are taken as the control objective.
2) The dynamic model of the DC microgrid under the proposed control is developed and steady-state analysis is performed to show that the control objectives can be achieved in steady state.
3) The performance of the proposed control is validated through real-time simulations on OPAL-RT.

The remainder of the paper is organized as follows. Section II introduces the cyber-physical model of the DC microgrid. The proposed unified distributed control is presented in Section III. Section IV develops the dynamic model of the DC microgrid under the proposed control and steady-state analysis is further presented in Section V. The performance of the proposed control is validated on a 8-DG DC microgrid in Section VI and conclusions are finally drawn in Section VII.

II. Cyber-Physical DC Microgrid

A. Physical Network of DC Microgrid

Assume there are N dispatchable DC sources, including N_1 GFM converters and N_2 GFE converters. All buses except the output buses of the DC sources are eliminated by Kron reduction. Let $\mathbf{Y}$ be the admittance matrix of the reduced network. Then the current injection vector of the DGs is:

$$\mathbf{i} = \mathbf{Y}\mathbf{v}, \tag{1}$$

where $\mathbf{i} = \left[\mathbf{i}_1^\top \, \mathbf{i}_2^\top\right]^\top$ with $\mathbf{i}_1 \in \mathbb{R}^{N_1}$ and $\mathbf{i}_2 \in \mathbb{R}^{N_2}$ as the current injection vectors respectively for GFM and GFE converters, $\mathbf{v} = \left[\mathbf{v}_1^\top \, \mathbf{v}_2^\top\right]^\top$ with $\mathbf{v}_1 \in \mathbb{R}^{N_1}$ and $\mathbf{v}_2 \in \mathbb{R}^{N_2}$ as the DG output voltage vectors for GFM and GFE converters. Let the Laplace transforms of $\mathbf{i}$ and $\mathbf{v}$ be $\mathbf{I}$ and $\mathbf{V}$, respectively, with $\mathbf{I} = \left[\mathbf{I}_1^\top \, \mathbf{I}_2^\top\right]^\top$ and $\mathbf{V} = \left[\mathbf{V}_1^\top \, \mathbf{V}_2^\top\right]^\top$.

B. Communication Network of DC Microgrid

A directed graph (digraph) $\mathcal{G}$ is used to model the communication network where nodes represent agents for the DGs and edges represent communication links between nodes. $\mathcal{G}$ can be represented by a time-invariant adjacency matrix $\mathbf{A} = [a_{ij}] \in \mathbb{R}^{N\times N}$. The Laplacian matrix is defined as $\mathbf{L} = \mathbf{D}^{\text{in}} - \mathbf{A}$ where $\mathbf{D}^{\text{in}} = \text{diag}\{d^{\text{in}}\}$ is the in-degree matrix with $d^{\text{in}} = \sum_{j\in\mathcal{N}_i} a_{ij}$ and $\mathcal{N}_i$ as the set of neighbors of node i. It is assumed that the Laplacian matrix is balanced and $\mathcal{G}$ has at least a spanning tree and minimum redundancy [8].

III. Unified Distributed Control of GFM and GFE Converters

The proposed distributed control is designed based on a distributed optimization problem. The following design objectives are considered:

1) The average voltage of the GFM and GFE converters should be regulated to the microgrid rated voltage;
2) The proportional current sharing among all GFM and GFE converters should be achieved.

Therefore, the following optimization problem is defined for DG i:

$$\min f_i, \tag{2}$$

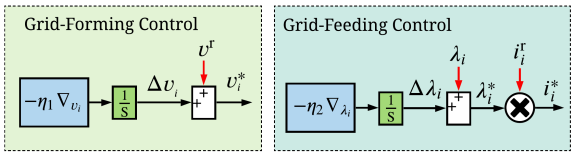

Fig. 1. Proposed unified distributed secondary control for GFM and GFE converters.

with $f_i = \frac{N\alpha}{2}(v^{\text{r}} - \bar{v})^2 + \frac{1}{2}\sum_{j\in\mathcal{N}_i} a_{ij}(\lambda_j - \lambda_i)^2 \triangleq f_i^1 + f_i^2$ where $\alpha > 0$ is a design parameter, $\bar{v} = \sum_{i=1}^N v_i/N$ is the average voltage of all converter output buses, v^{r} is the microgrid rated voltage, $\mathcal{N}_i$ is the set of the neighbors of DG i in $\mathcal{G}$, and $\lambda_i = i_i/i_i^{\text{r}}$ is the normalized current from DG i.

The average voltage $\bar{v}$ can be estimated by DG $i = 1, \cdots, N$ using a distributed average voltage observer [8]:

$$\overline{v}_i(t) = v_i(t) + \int_0^t \sum_{j\in\mathcal{N}_i} a_{ij}\big(\overline{v}_j - \overline{v}_i\big)d\tau, \tag{3}$$

where $\overline{v}_i$ is the estimated average voltage by DG i.

Differentiating (3) for $i = 1, \ldots, N$, the global average voltage observer dynamics can be obtained as:

$$\dot{\overline{\mathbf{v}}} = \dot{\mathbf{v}} - \mathbf{L}\overline{\mathbf{v}}, \tag{4}$$

where $\overline{\mathbf{v}} = \left[\overline{\mathbf{v}}_1^\top \, \overline{\mathbf{v}}_2^\top\right]^\top$ is the average voltage estimation vector. In frequency domain (4) becomes [8]:

$$\overline{\mathbf{V}} = s(s\boldsymbol{I}_N + \mathbf{L})^{-1}\mathbf{V} \triangleq \mathbf{G}\mathbf{V}, \tag{5}$$

where $\overline{\mathbf{V}} = \left[\overline{\mathbf{V}}_1^\top \, \overline{\mathbf{V}}_2^\top\right]^\top$ is the Laplace transform of $\overline{\mathbf{v}}$, $\boldsymbol{I}_N \in \mathbb{R}^{N\times N}$ is an identity matrix, and $\mathbf{G}$ is the distributed average voltage observer transfer-function matrix with $\mathbf{G}_1$ and $\mathbf{G}_2$ as the rows of $\mathbf{G}$ respectively corresponding to the GFM and GFE converters.

A. Secondary Control of GFM Converters

The secondary control in GFM converters generates voltage reference. The partial derivative of f_i with respect to v_i is:

$$\begin{aligned}\nabla_{v_i} \triangleq \frac{\partial f_i}{\partial v_i} &= \frac{\partial f_i^1}{\partial v_i} + \frac{\partial f_i^2}{\partial \lambda_i}\frac{\partial \lambda_i}{\partial i_i}\frac{\partial i_i}{\partial v_i} \\ &= \alpha\big(\overline{v}_i - v^{\text{r}}\big) - \frac{1}{i_i^{\text{r}}}\frac{\partial i_i}{\partial v_i}\sum_{j\in\mathcal{N}_i} a_{ij}(\lambda_j - \lambda_i).\end{aligned} \tag{6}$$

Since $\partial i_i/\partial v_i = Y_{ii}$ where Y_{ii} is the (i,i)th element of the bus admittance matrix $\mathbf{Y}$, (6) can be rewritten as:

$$\nabla_{v_i} = \alpha\big(\overline{v}_i - v^{\text{r}}\big) - \frac{Y_{ii}}{i_i^{\text{r}}}\sum_{j\in\mathcal{N}_i} a_{ij}(\lambda_j - \lambda_i). \tag{7}$$

Using (7) the voltage reference v_i^* for the GFM converter in an DC microgrid can be obtained as

$$v_i^* = v^{\text{r}} + \Delta_{v_i} \tag{8}$$

with $d\Delta_{v_i}/dt = -\eta_1\nabla_{v_i}$ where $\eta_1 > 0$ is a design parameter.

B. Secondary Control of GFE Converters

In GFE mode the secondary control generates current reference. The partial derivative of f_i with respect to λ_i is:

$$\begin{aligned}\nabla_{\lambda_i} \triangleq \frac{\partial f_i}{\partial \lambda_i} &= \frac{\partial f_i^1}{\partial v_i}\frac{\partial v_i}{\partial i_i}\frac{\partial i_i}{\partial \lambda_{i_i}} + \frac{\partial f_i^2}{\partial \lambda_i} \\ &= \alpha\frac{i_i^{\text{r}}}{Y_{ii}}\big(\overline{v}_i - v^{\text{r}}\big) - \sum_{j\in\mathcal{N}_i} a_{ij}(\lambda_j - \lambda_i).\end{aligned} \tag{9}$$

The current reference λ_i^* of DG i can be set as:

$$\lambda_i^* = \lambda_i + \Delta\lambda_i \tag{10}$$

with $d\Delta\lambda_i/dt = -\eta_2\nabla_{\lambda_i}$ where $\eta_2 > 0$ is a design parameter.

The block diagrams for the unified distributed control of GFM and GFE converters are shown in Fig. 1. When a DG is disconnected, its communication with its neighboring DGs becomes unavailable and it will not participate in average voltage regulation or current sharing. The average voltage of the remaining DGs will be regulated to the rated voltage and the current of the remaining DGs will be proportionally shared.

IV. DC Microgrid Dynamic Model

In the proposed control, $v^{\rm r}$ is the input whereas $\mathbf{V}$ and $\mathbf{I}$ are the outputs. Therefore, the dynamic model for the DC microgrid under the proposed control is developed to formulate the relationship between $v^{\rm r}$ and the outputs $\mathbf{V}$ and $\mathbf{I}$.

Let the vector of the partial derivatives of the objective function f_i with respect to the GFM DG voltages be $\nabla_1 = [\nabla_{v_1}, \nabla_{v_2}, \cdots, \nabla_{v_{N_1}}]^\top$ and its Laplace transform be $\boldsymbol{\nabla}_1$. Then in frequency domain (7) can be written as:

$$\boldsymbol{\nabla}_1 = \alpha\Big(\mathbf{G}_1\mathbf{V} - \frac{v^{\rm r}}{s}\mathbf{1}_{N_1}\Big) + \mathbf{H}_1\mathbf{L}_1\mathbf{I}^{{\rm r}^{-1}}\mathbf{I}, \tag{11}$$

where $\mathbf{1}_{N_1} \in \mathbb{R}^{N_1}$ is a column vector of all ones, $\mathbf{H}_1 = \text{diag}\{H_{1,i}\} \in \mathbb{R}^{N_1\times N_1}$ is defined for GFM converters with $H_{1,i} = Y_{ii}/i_i^{\rm r}$, $\mathbf{L}_1$ is obtained by only keeping the rows of $\mathbf{L}$ for GFM converters, and $\mathbf{I}^{\rm r} = \text{diag}\{i_i^{\rm r}\} \in \mathbb{R}^{N\times N}$.

Let the voltage references selected by the secondary control of GFM converters be $\mathbf{v}_1^* = [v_1^*, v_2^*, \cdots, v_{N_1}^*]^\top$. Accordingly in frequency domain (8) can be written as:

$$\mathbf{V}_1^* = \frac{v^{\rm r}}{s}\mathbf{1}_{N_1} + \alpha\mathbf{J}_1\Big(\mathbf{G}_1\mathbf{V} - \frac{v^{\rm r}}{s}\mathbf{1}_{N_1}\Big) + \mathbf{J}_1\mathbf{H}_1\mathbf{L}_1\mathbf{I}^{{\rm r}^{-1}}\mathbf{I}, \tag{12}$$

where $\mathbf{J}_1 = \text{diag}\{J_{1,i}\} \in \mathbb{R}^{N_1\times N_1}$ with $J_{1,i} = -\eta_1/s$.

Let the vector of the partial derivatives of the objective function f_i with respect to the GFE converter normalized currents be $\boldsymbol{\nabla}_2 = [\nabla_{\lambda_{N_1+1}}, \nabla_{\lambda_{N_1+2}}, \cdots, \nabla_{\lambda_N}]^\top$. Then in frequency domain (9) can be written as:

$$\boldsymbol{\nabla}_2 = \alpha\mathbf{H}_2\Big(\mathbf{G}_2\mathbf{V} - \frac{v^{\rm r}}{s}\mathbf{1}_{N_2}\Big) + \mathbf{L}_2\mathbf{I}^{{\rm r}^{-1}}\mathbf{I}, \tag{13}$$

where $\mathbf{H}_2 = \text{diag}\{H_{2,i}\} \in \mathbb{R}^{N_2\times N_2}$ with $H_{2,i} = i_{i+N_1}^{\rm r}/Y_{(i+N_1)(i+N_1)}$, $\mathbf{1}_{N_2} \in \mathbb{R}^{N_2}$, and $\mathbf{L}_2$ is obtained by only keeping the rows of $\mathbf{L}$ corresponding to the GFE converters.

Let the current references selected by the secondary control of the GFE converters be $\mathbf{i}_2^* = [i_{N_1+1}^*, i_{N_1+2}^*, \cdots, i_N^*]^\top$. Accordingly in frequency domain (10) can be written as:

$$\mathbf{I}_2^{\rm r}\mathbf{I}_2^* = \mathbf{I}_2^{\rm r}\mathbf{I}_2 + \alpha\mathbf{J}_2\mathbf{H}_2(\mathbf{G}_2\mathbf{V} - \frac{v^{\rm r}}{s}\mathbf{1}_{N_2}) + \mathbf{J}_2\mathbf{L}_2\mathbf{I}^{{\rm r}^{-1}}\mathbf{I}, \tag{14}$$

where $\mathbf{I}_2^{\rm r} = \text{diag}\{i_{i+N_1}^{\rm r}\} \in \mathbb{R}^{N_2\times N_2}$ and $\mathbf{J}_2 = \text{diag}\{J_{2,i}\} \in \mathbb{R}^{N_2\times N_2}$ with $J_{2,i} = -\eta_2/s$.

The input-output relationship for the DC-DC converter can be represented as [8]:

$$\mathbf{V}_1 = \mathbf{T}_1\mathbf{V}_1^* \tag{15}$$

$$\mathbf{I}_2 = \mathbf{T}_2\mathbf{I}_2^*, \tag{16}$$

where $\mathbf{T}_1 = \text{diag}\{T_{1,i}\} \in \mathbb{R}^{N_1\times N_1}$ and $\mathbf{T}_2 = \text{diag}\{T_{2,i}\} \in \mathbb{R}^{N_2\times N_2}$ are respectively the transfer-function matrices of the GFM and GFE converters.

Since in frequency domain (1) can be written as

$$\begin{bmatrix}\mathbf{I}_1\\ \mathbf{I}_2\end{bmatrix} = \begin{bmatrix}\mathbf{Y}_{11} & \mathbf{Y}_{12}\\ \mathbf{Y}_{21} & \mathbf{Y}_{22}\end{bmatrix}\begin{bmatrix}\mathbf{V}_1\\ \mathbf{V}_2\end{bmatrix}, \tag{17}$$

we can get

$$\mathbf{V}_2 = \mathbf{Y}_{22}^{-1}(\mathbf{I}_2 - \mathbf{Y}_{21}\mathbf{V}_1) \tag{18}$$

$$\mathbf{I}_1 = \mathbf{Y}_{11}\mathbf{V}_1 + \mathbf{Y}_{12}\mathbf{Y}_{22}^{-1}(\mathbf{I}_2 - \mathbf{Y}_{21}\mathbf{V}_1). \tag{19}$$

Then from (18) we have

$$\mathbf{V} = \begin{bmatrix}\mathbf{V}_1\\ \mathbf{V}_2\end{bmatrix} = \begin{bmatrix}\mathbf{0}_{N_1}\\ \mathbf{Y}_{22}^{-1}\mathbf{I}_2\end{bmatrix} + \begin{bmatrix}\boldsymbol{I}_{N_1}\\ -\mathbf{Y}_{22}^{-1}\mathbf{Y}_{21}\end{bmatrix}\mathbf{V}_1 \triangleq \mathbf{B}_0 + \mathbf{B}_1\mathbf{V}_1, \tag{20}$$

where $\mathbf{0}_{N_1} \in \mathbb{R}^{N_1}$ is a vector with all zeros.

Substituting (12) and (20) into (15) we can get:

$$\mathbf{C}_1\mathbf{V}_1 + \mathbf{C}_2\mathbf{I}_2 = \mathbf{C}_0, \tag{21}$$

where $\mathbf{C}_0 = -v^{\rm r}\mathbf{T}_1(\boldsymbol{I}_{N_1} - \alpha\mathbf{J}_1)\mathbf{1}_{N_1}/s$, $\mathbf{C}_1 = \mathbf{D}\mathbf{B}_1 - \boldsymbol{I}_{N_1}$, $\mathbf{C}_2 = \mathbf{D}_2\mathbf{Y}_{22}^{-1}$, and $\mathbf{D} = \mathbf{T}_1\mathbf{J}_1(\alpha\mathbf{G}_1 + \mathbf{H}_1\mathbf{L}_1\mathbf{I}^{{\rm r}^{-1}}\mathbf{Y}) \triangleq [\mathbf{D}^1\,\mathbf{D}^2]$ with $\mathbf{D}^1 \in \mathbb{R}^{N_1\times N_1}$ and $\mathbf{D}^2 \in \mathbb{R}^{N_1\times N_2}$.

Similarly, substituting (14) and (20) into (16) we can get:

$$\mathbf{E}_1\mathbf{V}_1 + \mathbf{E}_2\mathbf{I}_2 = \mathbf{E}_0, \tag{22}$$

where $\mathbf{E}_0 = \alpha v^{\rm r}\mathbf{T}_2\mathbf{I}_2^{{\rm r}^{-1}}\mathbf{J}_2\mathbf{H}_2\boldsymbol{I}_{N_2}/s$, $\mathbf{E}_1 = \mathbf{F}_1\mathbf{B}_1$, $\mathbf{E}_2 = \mathbf{F}_2 + \mathbf{F}_1^2\mathbf{Y}_{22}^{-1} - \boldsymbol{I}_{N_2}$, $\mathbf{F}_1 = \mathbf{T}_2\mathbf{I}_2^{{\rm r}^{-1}}\mathbf{J}_2(\alpha\mathbf{H}_2\mathbf{G}_2 + \mathbf{L}_2\mathbf{I}^{{\rm r}^{-1}}\mathbf{Y}) \triangleq [\mathbf{F}_1^1\,\mathbf{F}_1^2]$ with $\mathbf{F}_1^1 \in \mathbb{R}^{N_2\times N_1}$ and $\mathbf{F}_1^2 \in \mathbb{R}^{N_2\times N_2}$, and $\mathbf{F}_2 = \mathbf{T}_2\mathbf{I}_2^{{\rm r}^{-1}}\mathbf{I}_2^{\rm r}$.

Finally solving (21) and (22) we get:

$$\mathbf{V}_1 = (\mathbf{C}_1 + \mathbf{C}_2\mathbf{E}_2^{-1}\mathbf{E}_1)^{-1}(\mathbf{C}_0 - \mathbf{C}_2\mathbf{E}_2^{-1}\mathbf{E}_0) \tag{23}$$

$$\mathbf{I}_2 = (\mathbf{E}_2^{-1}\mathbf{E}_1\mathbf{C}_1^{-1}\mathbf{C}_2 - \boldsymbol{I}_{N_2})^{-1}\mathbf{E}_2^{-1}(\mathbf{E}_1\mathbf{C}_1^{-1}\mathbf{C}_0 - \mathbf{E}_0). \tag{24}$$

Then we can also obtain $\mathbf{V}_2$ and $\mathbf{I}_1$ respectively from (18) and (19) based on (23) and (24).

V. Steady-State Analysis

In this section we perform steady-state analysis and show that all objectives can be achieved by the proposed control. From (12), (14), and (15)–(16) in Section IV we can get:

$$\mathbf{V}_1 = \mathbf{T}_1\Bigg(\frac{v^{\rm r}}{s}\mathbf{1}_{N_1} + \alpha\mathbf{J}_1\Big(\overline{\mathbf{V}}_1 - \frac{v^{\rm r}}{s}\mathbf{1}_{N_1}\Big) + \mathbf{J}_1\mathbf{H}_1\mathbf{L}_1\mathbf{I}^{{\rm r}^{-1}}\mathbf{I}\Bigg) \tag{25}$$

$$\mathbf{I}_2 = \mathbf{T}_2\Bigg(\mathbf{I}_2 + \alpha\mathbf{I}_2^{{\rm r}^{-1}}\mathbf{J}_2\mathbf{H}_2\Big(\overline{\mathbf{V}}_2 - \frac{v^{\rm r}}{s}\mathbf{1}_{N_2}\Big) + \mathbf{I}_2^{{\rm r}^{-1}}\mathbf{J}_2\mathbf{L}_2\mathbf{I}^{{\rm r}^{-1}}\mathbf{I}\Bigg). \tag{26}$$

Applying final value theorem on (25) we have

$$\lim_{s\to 0} s\mathbf{T}_1^{-1}\mathbf{v}_1^{\rm ss} = \lim_{s\to 0} sv^{\rm r}\mathbf{1}_{N_1} + \alpha\lim_{s\to 0} s\mathbf{J}_1(\overline{\mathbf{v}}_1^{\rm ss} - v^{\rm r}\mathbf{1}_{N_1}) + \lim_{s\to 0} s\mathbf{J}_1\mathbf{H}_1\mathbf{L}_1\mathbf{I}^{{\rm r}^{-1}}\mathbf{i}^{\rm ss}, \tag{27}$$

where $\mathbf{v}_1^{\rm ss}$ is the steady-state voltage vector for GFM converters, $\overline{\mathbf{v}}_1^{\rm ss}$ is the vector of the steady-state average voltage estimates of GFM converters, and $\mathbf{i}^{\rm ss}$ is the steady-state vector for current injections of all converters.

When the communication network of the DC microgrid has at least a spanning tree and a balanced Laplacian matrix, the steady-state average voltage estimated by all DG converters, $\overline{\mathbf{v}}^{\rm ss}$, will converge to the true average-voltage i.e. $\overline{\mathbf{v}}^{\rm ss} =$

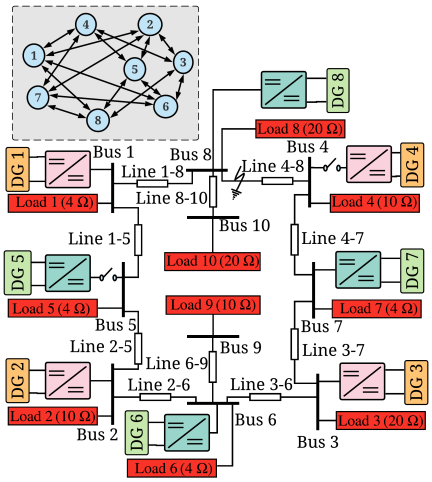

Fig. 2. Schematic diagram of the 8-DG DC microgrid test system and the communication network.

$\langle \mathbf{v}^{\rm ss} \rangle \mathbf{1}_N$ where $\langle \mathbf{v}^{\rm ss} \rangle$ is the average of all elements in $\mathbf{v}^{\rm ss}$ [8]. Since the DC-gain of the closed-loop DC-DC converters is equal to one [8], we have $\lim_{s\to 0} \mathbf{T}_1 = \lim_{s\to 0} \mathbf{T}_1^{-1} = \boldsymbol{I}_{N_1}$. Also note that $\lim_{s\to 0} s\boldsymbol{I}_{N_1} = \mathbf{0}_{N_1\times N_1}$, $\lim_{s\to 0} s\mathbf{1}_{N_1} = \mathbf{0}_{N_1}$, and $\lim_{s\to 0} s\mathbf{J}_1 = \tilde{\mathbf{J}}_1 = \text{diag}\{\tilde{J}_{1,i}\} \in \mathbb{R}^{N_1\times N_1}$ with $\tilde{J}_{1,i} = -\eta_1$ [8]. Then (27) can be simplified as

$$\alpha \tilde{\mathbf{J}}_1 \big(\langle \mathbf{v}^{\rm ss} \rangle - v^{\rm r}\big)\mathbf{1}_{N_1} = -\tilde{\mathbf{J}}_1 \mathbf{H}_1 \mathbf{L}_1 {\mathbf{I}^{\rm r}}^{-1} \mathbf{i}^{\rm ss}. \tag{28}$$

Since $\mathbf{1}^\top \mathbf{L} = \mathbf{0}_N^\top$, $\alpha > 0$, and all diagonal elements of the diagonal matrix $\mathbf{H}_1$ are nonzero, premultiplying both sides of (28) by $\mathbf{1}_{N_1}^\top \mathbf{H}_1^{-1} \tilde{\mathbf{J}}_1^{-1}$ we have

$$\big(\langle \mathbf{v}^{\rm ss} \rangle - v^{\rm r}\big) \sum_{i=1}^{N_1} H_{1,i}^{-1} = 0. \tag{29}$$

Because $H_{1,i} > 0$ for $i = 1, \ldots, N_1$, from (29) we have $\langle \mathbf{v}^{\rm ss} \rangle = v^{\rm r}$, implying that the proposed control can successfully regulate the average voltage of all converters to be the rated voltage. Further substituting (29) into (28) we can obtain

$$\mathbf{L}_1 {\mathbf{I}^{\rm r}}^{-1} \mathbf{i}^{\rm ss} = \mathbf{0}_{N_1}. \tag{30}$$

Similarly, applying final value theorem on (26) we have

$$\lim_{s\to 0} s\mathbf{T}_2^{-1}\mathbf{i}_2^{\rm ss} = \lim_{s\to 0} s\mathbf{i}_2^{\rm ss} + \alpha \lim_{s\to 0} s{\mathbf{I}_2^{\rm r}}^{-1}\mathbf{J}_2\mathbf{H}_2(\overline{\mathbf{v}}_2^{\rm ss} - v^{\rm r}\mathbf{1}_{N_2}) + \lim_{s\to 0} s{\mathbf{I}_2^{\rm r}}^{-1}\mathbf{J}_2\mathbf{L}_2{\mathbf{I}^{\rm r}}^{-1}\mathbf{i}^{\rm ss}, \tag{31}$$

where $\mathbf{v}_2^{\rm ss}$ and $\mathbf{i}_2^{\rm ss}$ are, respectively, the steady-state voltage and current injection vectors for GFE converters, and $\overline{\mathbf{v}}_2^{\rm ss}$ is the vector of the steady-state average voltage estimates of GFE converters. For the DC-DC converters, we have $\lim_{s\to 0} \mathbf{T}_2 = \lim_{s\to 0} \mathbf{T}_2^{-1} = \boldsymbol{I}_{N_2}$. Since $\lim_{s\to 0} s\boldsymbol{I}_{N_2} = \mathbf{0}_{N_2\times N_2}$, $\lim_{s\to 0} s\mathbf{1}_{N_2} = \mathbf{0}_{N_2}$, $\lim_{s\to 0} s\mathbf{J}_2 = \tilde{\mathbf{J}}_2 = \text{diag}\{\tilde{J}_{2,i}\} \in \mathbb{R}^{N_2\times N_2}$ with $\tilde{J}_{2,i} = -\eta_2$ [8], and $\overline{\mathbf{v}}_2^{\rm ss} - v^{\rm r}\mathbf{1}_{N_2} = \big(\langle \mathbf{v}^{\rm ss} \rangle - v^{\rm r}\big)\mathbf{1}_{N_2} = \mathbf{0}_{N_2}$, (31) can be simplified as:

$${\mathbf{I}_2^{\rm r}}^{-1}\tilde{\mathbf{J}}_2\mathbf{L}_2{\mathbf{I}^{\rm r}}^{-1}\mathbf{i}^{\rm ss} = \mathbf{0}. \tag{32}$$

Premultiplying both sides of (32) by $\mathbf{1}_{N_2}^\top \tilde{\mathbf{J}}_2^{-1}\mathbf{I}_2^{\rm r}$ we have

$$\mathbf{L}_2 {\mathbf{I}^{\rm r}}^{-1} \mathbf{i}^{\rm ss} = \mathbf{0}_{N_2}. \tag{33}$$

From (30) and (33) it is clear that $\mathbf{L}{\mathbf{I}^{\rm r}}^{-1}\mathbf{i}^{\rm ss} = \mathbf{0}_N$ which means all converters will achieve proportional current sharing.

TABLE I
PARAMETERS OF THE TEST SYSTEM

	Parameters		Value
	Symbol	Quantity	
DGs	$v^{\rm r}$	Rated voltage	48V
	$i_1^{\rm r}$, $i_3^{\rm r}$, $i_5^{\rm r}$, $i_7^{\rm r}$	DG1, DG3, DG5, DG7 rated current	12 A
	$i_2^{\rm r}$, $i_4^{\rm r}$, $i_6^{\rm r}$, $i_8^{\rm r}$	DG2, DG4, DG6, DG8 rated current	15 A
Lines	$R_{1\text{-}8}, R_{4\text{-}8}, R_{2\text{-}6}, R_{3\text{-}6}$	Line resistance	0.75 Ω
	$L_{1\text{-}8}, L_{4\text{-}8}, L_{2\text{-}6}, L_{3\text{-}6}$	Line inductance	7.5 µH
	$R_{1\text{-}5}, R_{3\text{-}7}, R_{4\text{-}7}$	Line resistance	0.85 Ω
	$L_{1\text{-}5}, L_{3\text{-}7}, L_{4\text{-}7}$	Line inductance	8.5 µH
	$R_{8\text{-}10}, R_{6\text{-}9}$	Line resistance	0.5 Ω
	$L_{8\text{-}10}, L_{6\text{-}9}$	Line inductance	5 µH
	$R_{2\text{-}5}$	Line resistance	1 Ω
	$L_{2\text{-}5}$	Line inductance	10 µH

VI. Real-Time Simulation Results

The performance of the proposed unified distributed control is validated through real-time simulation on an 8-DG DC microgrid test system shown in Fig. 2. The parameters of the test system are given in Table I where converters for Source 1–Source 4 are considered as GFM converters and those for Source 5–Source 6 are as GFE converters. The topology of the communication network is also shown in Fig. 2. We set $a_{ij} = 1$ in $\mathbf{A}$ if there is a communication link between nodes i and j, and $a_{ij} = 0$ otherwise. The real-time simulations are performed at 50 µs time step using the ODE-5 solver on OPAL-RT OP4510. The parameters α, η_1, and η_2 are respectively selected as 1, 2, and 2.

A. Performance Under Load Changes

Fig. 3 shows the control performance under load changes. Initially the system is operating under the load condition shown in Fig. 2 except that the load at Bus 9 is disconnected. Then at 10 s and 40 s, respectively, a 20 Ω and 10 Ω load are connected to Bus 9. Due to the impact of the load changes the system operating conditions change. Fig. 3a shows that the proposed control successfully achieves the objective of average voltage regulation among all GFM and GFE converters and the average value of the output buses of all converters is regulated to the rated voltage (1 p.u.). Fig. 3b shows that the proposed control achieves proportional current sharing among all GFM and GFE converters. In Fig. 3c it is seen that the average voltage that is distributedly estimated by each DG can converge to the actual average voltage.

B. Performance Under Disconnection of Sources and Lines

Fig. 4 demonstrates the control performance when a GFE converter at DG 5 and GFM converter at DG 4 are disconnected from the DC microgrid, respectively at 10 s and 40 s. Due to the disconnection, the communication links of the disconnected DGs become unavailable and the disconnected DGs will not participate in voltage regulation or current sharing. After a DG is disconnected the voltage at that bus experiences a sag, due to which the global average voltage becomes less than the microgrid rated voltage (see $\bar{v}$ in Fig. 4a). However, the average voltage of the remaining DGs can still be regulated to the rated voltage (see $\bar{v}'$ in Fig. 4a). After

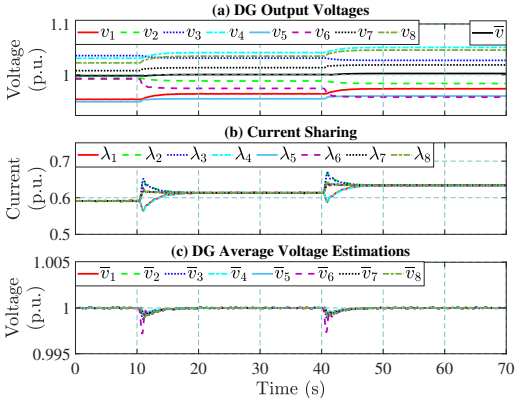

Fig. 3. Performance under load changes applied at 10 s and 40 s.

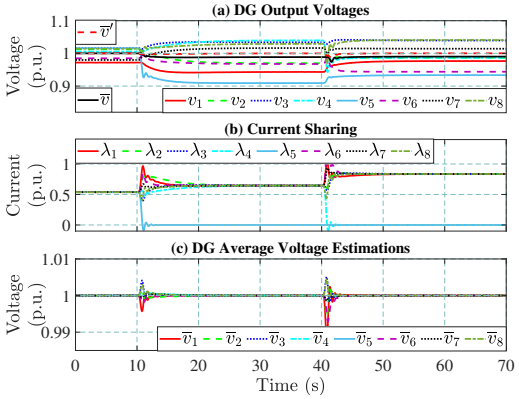

Fig. 4. Performance when Source 5 is disconnected at 10 s and Source 4 is disconnected at 40 s. Note that $\overline{v}'$ in (a) is the average voltage of the remaining DGs. After a DG is disconnected it will not estimate the average voltage and thus in (c) the estimation result is not shown after a DG is disconnected.

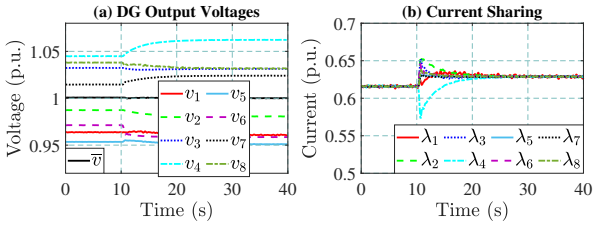

Fig. 5. Performance when Line 4-8 is disconnected at 10 s due to a fault.

a DG is disconnected from a bus, the current injection from that DG becomes zero, but the remaining DGs can still achieve proportional current sharing, as seen in Fig. 4b.

Fig. 5 shows the control performance when Line 4-8 is disconnected due to a fault. Despite this disturbance, the physical network remains connected. It is seen that the proposed control can still achieve both voltage regulation and proportional current sharing objectives and can still work well under disconnection of sources or lines.

Note that the proposed control does not incorporate fault ride-through capabilities in the control design. However, it is possible to adapt and incorporate a fault ride-through scheme such as the one in [14] into the control design to inject fault current in case of temporary faults.

VII. Conclusion

In this paper, we propose a unified distributed control for the GFM and GFE converters in DC microgrids. The secondary control of both GFM and GFE converters is designed based on a set of formulated optimization problems in order to optimally coordinate two types of converters for voltage regulation and current sharing. The control structure is similar for both GFM and GFE converters which will facilitate implementation in real systems. Steady-state analysis of the proposed control shows that all control objectives can be achieved for two types of converters. From the OPAL-RT based real-time simulation results, it is also clearly seen that the proposed control successfully achieves the desired control objectives on average voltage regulation and proportional current sharing among all GFM and GFE converters.

References

[1] S. Sahoo and S. Mishra, "An adaptive event-triggered communication-based distributed secondary control for dc microgrids," *IEEE Trans. Smart Grid*, vol. 9, no. 6, pp. 6674–6683, Jun. 2018.

[2] P. Prabhakaran, Y. Goyal, and V. Agarwal, "Novel nonlinear droop control techniques to overcome the load sharing and voltage regulation issues in dc microgrid," *IEEE Trans. Power Electron.*, vol. 33, no. 5, pp. 4477–4487, May. 2018.

[3] R. Han, H. Wang, Z. Jin, L. Meng, and J. M. Guerrero, "Compromised controller design for current sharing and voltage regulation in dc microgrid," *IEEE Trans. Power Electron.*, vol. 34, no. 8, pp. 8045–8061, Aug. 2019.

[4] P. Prabhakaran, Y. Goyal, and V. Agarwal, "A novel communication-based average voltage regulation scheme for a droop controlled dc microgrid," *IEEE Trans. Smart Grid*, vol. 10, no. 2, pp. 1250–1258, Mar. 2019.

[5] T. Dragičević, J. M. Guerrero, J. C. Vasquez, and D. Škrlec, "Supervisory control of an adaptive-droop regulated dc microgrid with battery management capability," *IEEE Trans. Power Electron.*, vol. 29, no. 2, pp. 695–706, Feb. 2014.

[6] M. S. Sadabadi, Q. Shafiee, and A. Karimi, "Plug-and-play robust voltage control of DC microgrids," *IEEE Trans. Smart Grid*, vol. 9, no. 6, pp. 6886–6896, Nov. 2018.

[7] S. M. Mohiuddin and J. Qi, "Droop-free distributed control for AC microgrids with precisely regulated voltage variance and admissible voltage profile guarantees," *IEEE Trans. Smart Grid*, vol. 11, no. 3, pp. 1956–1967, May 2020.

[8] V. Nasirian, S. Moayedi, A. Davoudi, and F. L. Lewis, "Distributed cooperative control of DC microgrids," *IEEE Trans. Power Electron.*, vol. 30, no. 4, pp. 2288–2303, Apr. 2015.

[9] R. Bhattarai, J. Qi, J. Wang, and S. Kamalasadan, "Adaptive droop control of coupled microgrids for enhanced power sharing and small-signal stability," in *2020 IEEE Power Energy Society General Meeting (PESGM)*, Aug. 2020, pp. 1–5.

[10] S. M. Mohiuddin and J. Qi, "A unified droop-free distributed secondary control for grid-following and grid-forming inverters in AC microgrids," in *IEEE Power and Energy Society General Meeting*, 2020.

[11] H. Sun, Q. Guo, J. Qi, V. Ajjarapu, R. Bravo, J. Chow, Z. Li, R. Moghe, E. Nasr-Azadani, U. Tamrakar *et al.*, "Review of challenges and research opportunities for voltage control in smart grids," *IEEE Trans. Power Syst.*, Jul. 2019.

[12] S. M. Mohiuddin and J. Qi, "Attack resilient distributed control for ac microgrids with distributed robust state estimation," in *2021 IEEE Texas Power and Energy Conference (TPEC)*, Feb. 2021, pp. 1–6.

[13] R. Han, M. Tucci, A. Martinelli, J. M. Guerrero, and G. Ferrari-Trecate, "Plug-and-play voltage/current stabilization dc microgrid clusters with grid-forming/feeding converters," in *2018 Annual American Control Conference (ACC)*, Jun. 2018, pp. 5362–5367.

[14] X. Liu, C. Li, M. Shahidehpour, Y. Gao, B. Zhou, Y. Zhang, J. Yi, and Y. Cao, "Fault current hierarchical limitation strategy for fault ride-through scheme of microgrid," *IEEE Trans. Smart Grid*, vol. 10, no. 6, pp. 6566–6579, Nov. 2019.